Living Star Polymer Formation: Detailed Assessment of Poly(acrylate) Radical Reaction Pathways via ESI-MS

Gene Hart-Smith, Hugh Chaffey-Millar, and Christopher Barner-Kowollik*

Centre for Advanced Macromolecular Design, School of Chemical Sciences and Engineering, The University of New South Wales, Sydney NSW 2052, Australia

Received November 15, 2007; Revised Manuscript Received January 22, 2008

ABSTRACT: The generation of star polymers via living polymerization protocols is well documented; however, the impact of midchain radicals (MCRs) on the precise formation pathways under operation in living acrylate star polymerizations is still poorly understood. In the present study, electrospray ionization–mass spectrometry (ESI-MS) technology has been applied to map the products generated in R-group approach reversible addition fragmentation chain transfer (RAFT) methyl acrylate (MA) star polymerizations in order to gain insight into the precise formation pathways under operation in such systems. The polymerizations were conducted at 65 °C using the tetrafunctional RAFT agent 1,2,4,5-tetrakis(2-phenylthioacetylsulfanylmethyl)benzene and 2,2′-azobis(isobutyronitrile) (AIBN) as the thermally decomposing initiator. Initiator fragment derived linear chains, ideal stars, star–star couples, and other terminated star products formed as a result of combination and disproportionation reactions were successfully imaged. Additionally, MCR derived products that lie outside of the conventional R-group approach RAFT star polymerization mechanistic scheme were identified. Products associated with termination reactions involving intermolecularly formed MCRs on star arms and linear chains were observed; specifically, structures formed from MCR termination with propagating stars or radical carrying star cores, or with initiator fragments or propagating initiator derived linear chains. Additionally, structures produced via repropagation of intermolecularly formed MCRs on star arms were also identified. The products generated from MCR-derived reaction pathways were imaged from a degree of polymerization (DP_n) as low as one, indicating that MCRs can form upon molecules carrying only a single monomer unit.

Introduction

The manufacture of complex macromolecular architectures has been revolutionized by the advent of "living" free radical polymerization protocols, which allow for precise control of the degree of polymerization while generating materials of a low polydispersity. Of particular interest is the capability of these techniques to generate well-defined star polymer structures, which opens an additional avenue by which polymer properties may be carefully tuned.[1,2] The most prominent of these living free radical polymerization methodologies are atom transfer radical polymerizations (ATRP),[3–6] nitroxide-mediated polymerizations (NMP),[7,8] and the reversible addition–fragmentation chain transfer (RAFT) process.[9,10] When using ATRP and NMP methodologies to generate star polymers, the macromolecular scaffold[11] is always a radical carrying species, whereas two distinct approaches to the design of star polymer architectures are possible when using RAFT, these approaches being termed Z-group and R-group approach polymerizations. In R-group approach polymerizations (depicted in Scheme 1), the dithioester moiety leaves the scaffold structure and mediates the polymerization disconnected from the core, leaving the core itself to carry a radical in a similar manner to ATRP and NMP star polymerizations. In contrast, the Z-group technique operates on the principle that the RAFT agent stays tethered to the central macromolecular scaffold. This has the important consequence that the core will not carry propagating radical functions, as propagation occurs exclusively in the solution surrounding the core. In principle, Z-group polymerizations therefore offer the opportunity to generate extremely well-defined star polymer products up to high monomer to polymer conversions without the added complexity of cross coupling reactions;[12,13] a design feature that is not achievable when using ATRP, NMP, or R-group approach RAFT polymerizations due to the ever-present potential for the radical carrying core to undergo coupling reactions. However, these latter techniques can still be extremely well suited to the manufacture of highly defined complex polymer architectures when the reaction conditions employed in these methodologies are finely tuned.[14–17] When working under the constraints of specific monomers and reaction conditions, firm guiding principles are therefore a necessity if rational choices of design methodology are to be made.

In order to better understand the mechanistic underpinnings behind such living star polymerizations, several studies on systems that can produce highly structured molecular weight distributions (MWDs) have been undertaken by Barner-Kowollik and co-workers.[18–20] For example, in addition to ideal star material, R-group approach styrene star polymerizations have been shown to produce lower molecular weight polymer products, in addition to large, broad higher molecular weight shoulders on the MWDs resulting from these polymerizations.[17,20] Using a combined theoretical and experimental approach, it was concluded that the formation of initiator fragment derived linear chains and star–star couples[21] can serve to explain these highly structured MWDs.[20] The presence of these materials was unambiguously established through the use of mass spectrometry techniques on similar *p*-acetoxystyrene (AcOSty) R-group approach systems,[19] confirming that these products can play an important role in the generation of complex MWDs in living star systems.

These previous studies had focused on R-group approach RAFT polymerizations featuring monomers in which midchain radical (MCR) formation is not known to be pronounced; however, a significant degree of added complexity would be expected from living star polymerizations of acrylate monomers. It is widely accepted that MCRs play a significant role in the deviation of acrylate polymerizations from the ideal free radical polymerization reaction scheme,[22–26] and it has been indicated that the formation of MCRs can have a considerable impact upon the MWDs of controlled radical polymerizations.[27–29] MCRs are increasingly formed from temperatures as low as −40
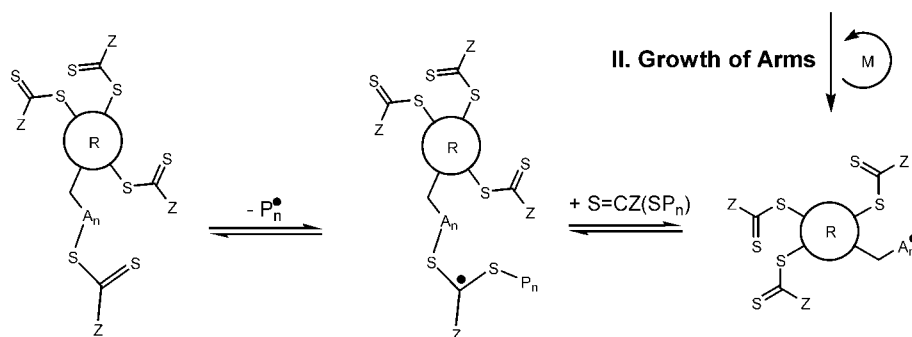
* Corresponding author: Tel +61 2 9385 4331, fax +61 2 9385 6250, e-mail c.barner-kowollik@unsw.edu.au.

Scheme 1. Conventional R-Group Approach RAFT Polymerization Mechanistic Scheme, in Which MCR Formation Is Not Considered[a]
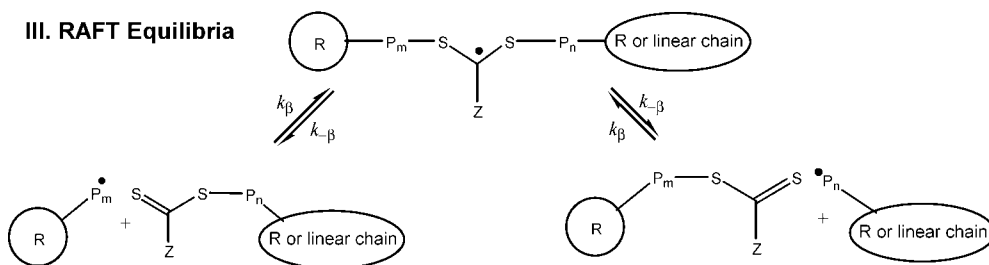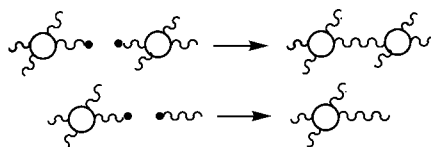
I. RAFT Group Activation
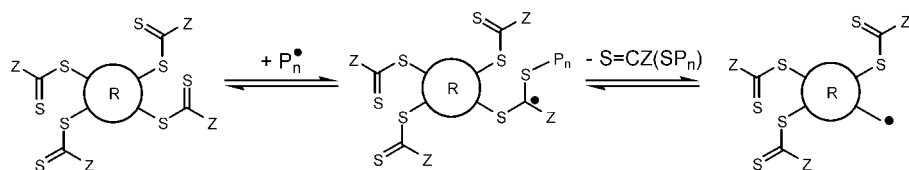
II. Growth of Arms

III. RAFT Equilibria

IV. Star Termination Reactions

[a] Star arm growth takes place on the star scaffold proper; RAFT equilibria take place between stars and stars, stars and linear chains, and linear chains and linear chains.

°C onward[30] via transfer reactions in which the radical functionality of the secondary propagating radical (SPR) is transferred to the polymer backbone via an H-shift reaction.[31–38] Such transfer reactions may proceed via intramolecular "back-biting" reactions, in which a [1,5] H-shift reaction is favored to occur, or via intermolecular pathways. The resulting MCRs may then terminate with other radical species (e.g., reaction pathway III of Scheme 2), undergo propagation at a significantly reduced rate (e.g., reaction pathway IV of Scheme 2), take part in transfer reactions with a chain-transfer agent (CTA) (e.g., reaction pathway V of Scheme 2), or undergo β-scission reactions in which shortened macroradicals and unsaturated dead polymer are produced (e.g., reaction pathways I and II of Scheme 2).[25,36,39] In an acrylate star polymerization system, multiple star arms and/or linear chains may conceivably be involved in such reaction pathways, adding complexity to the mechanistic processes involved. Indeed, Boschmann and Vana observed high molecular weight components in Z-group approach RAFT polymerizations of acrylates,[27] components which are not in accordance with the conventional Z-group approach RAFT polymerization mechanistic scheme. These authors attributed these products to star−star couples formed via intermolecular chain transfer to polymer reactions, demonstrating the extent to which long-chain branching can impact acrylate star polymerizations.

In this present contribution, electrospray ionization mass spectrometry (ESI-MS) is employed to map the products generated in R-group approach RAFT methyl acrylate (MA) polymerizations. It has been well documented that mass spectrometry techniques, such as matrix-assisted laser desorption and ionization-time-of-flight-mass spectrometry (MALDI-TOF-MS) and ESI-MS, are powerful methods in the analysis of synthetic polymers.[41–47] Such mass spectrometry methodologies can allow the structural details of individual polymer chains to be mapped with a high degree of accuracy and sensitivity, allowing insights to be gained into, for example, chain initiation and termination mechanisms.[48–51] ESI-MS is a particularly soft ionization technique, capable of imaging products with virtually no chain or end-group fragmentation.[24,48–56] Herein, a detailed map of the products produced in R-group approach RAFT MA star polymerizations has been generated for the first time using ESI-MS techniques, thereby allowing insights to be gained into the precise formation processes under operation in acrylate star polymerizations.

Scheme 2. Various Reaction Pathways Available to MCRs Formed on Living Chains in R-Group Approach RAFT MA Star Polymerizations[40] *a*
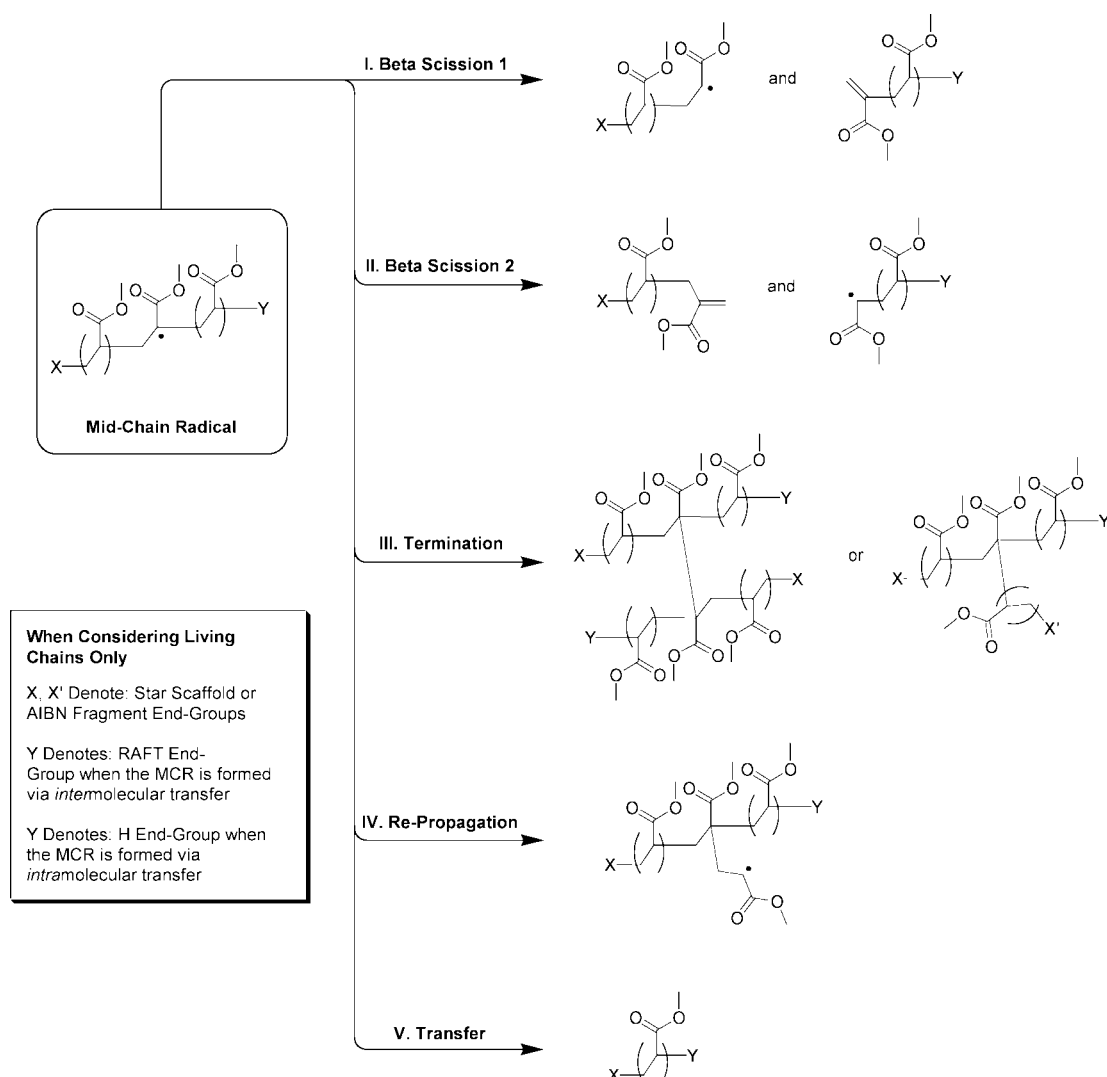
a Such reaction pathways are also available to MCRs formed on dead chains via intermolecular transfer reactions. Repeating monomer units have been enclosed in parentheses.

Experimental Section

Materials. Methyl acrylate (Aldrich, 99%) was deinhibited by passing through a column of basic alumina prior to use. 2,2′-Azobis(isobutyronitrile) (AIBN) (DuPont) was recrystallized two times from ethanol prior to use. Toluene (Ajax, analytical grade) was used as received. The synthesis of 1,2,4,5-tetrakis(phenylthioacetylsulfanylmethyl)benzene (4-arm RAFT agent) has been described elsewhere.[20] 300 MHz ^{1}H NMR (CDCl$_3$) analysis of the purified RAFT agent gave δ [ppm] = 4.27 (s, 8H), 4.29 (s, 8H), 7.16 (s, 2H), 7.21–7.36 (m, 20H). Careful inspection of the spectrum revealed no impurities.
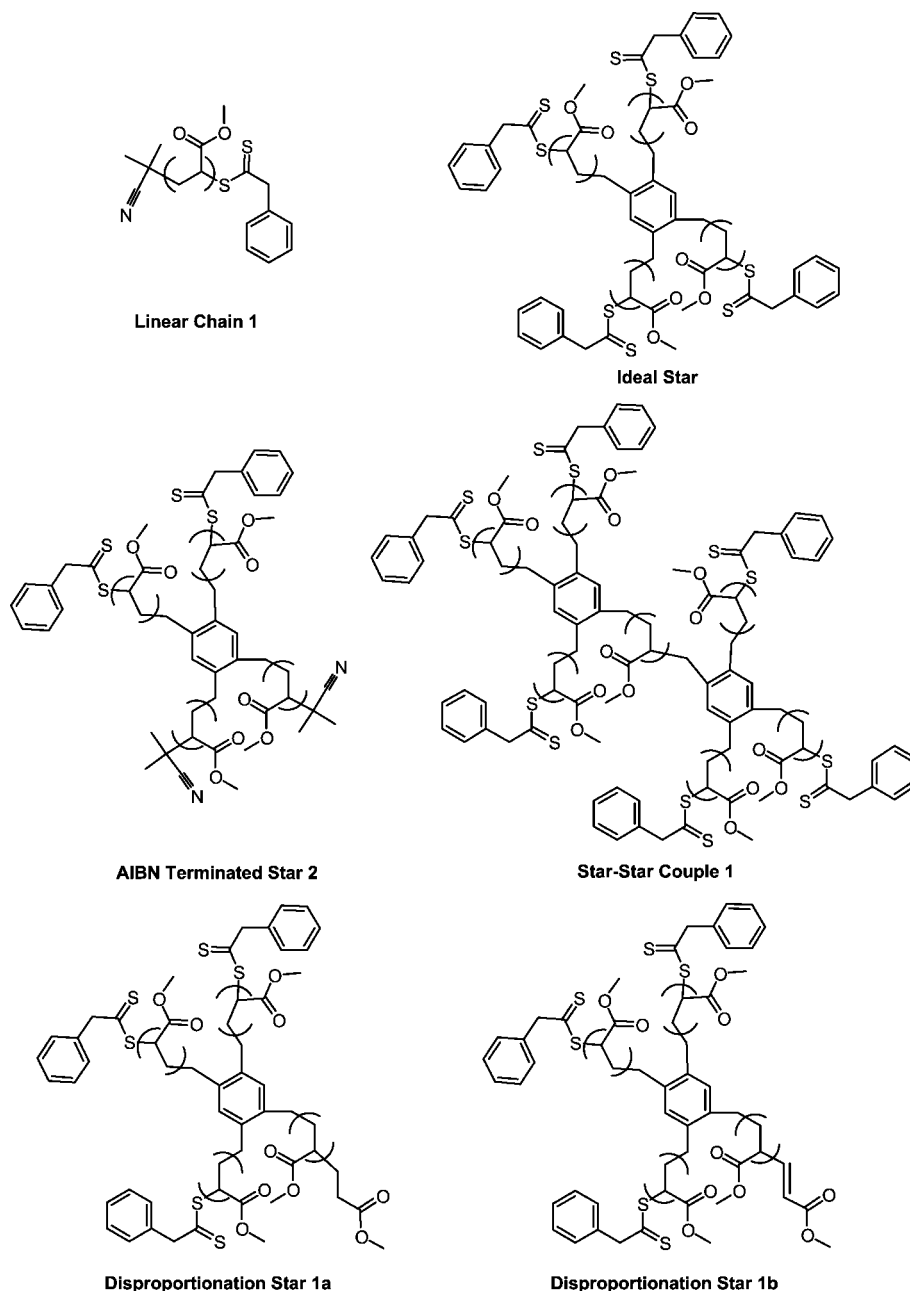
Polymerization Procedure. A typical polymerization involved adding a 10/90 vol % MA/toluene solution to a 10 mL volumetric flask containing 80 mg of 4-arm RAFT agent (1×10^{-2} mol L^{-1}) and 16 mg of AIBN (1×10^{-2} mol L^{-1}). 2 mL portions of the reaction mixture were transferred to glass ampules, which were sealed with rubber septa and copper wire. The solutions were then deoxygenated via N$_2$ purging for no less than 15 min. Ampules were placed in an oil bath at 65 °C, and samples prepared for ESI-MS analysis were typically removed after 240 min. After removal from the oil bath, the samples were immediately quenched in ice–water.

Monomer to polymer conversions typically reached orders of a few percent, and thus, accurate conversion data were difficult to obtain. This bears little consequence to the aims of the present study,

as observations of the formation pathways operative in the system under investigation are only dependent on the polymer end-group functionalities.

Mass Spectrometry Analysis. By identifying the product ions formed during ESI-MS analyses, detailed maps of the products produced during R-group approach RAFT MA star polymerizations may be obtained. In order to identify these product ions, structural libraries were created for the possible product species generated in the star polymer system under investigation (see the Results and Discussion section for further elaboration). All theoretical molecular weights were calculated using the exact mass as provided by the software package CS ChemDraw Ultra version 5.0 for the lightest isotope of the product of interest. Theoretical isotopic peak patterns were generated using the software package Xcalibur version 1.4.

A Thermo Finnigan LCQ Deca ion trap mass spectrometer (Thermo Finnigan, San Jose, CA) was employed in the MS studies. The LCQ Deca ion trap instrument was equipped with an atmospheric pressure ionization source operating in the nebulizer-assisted electrospray mode and was used in positive ion mode. Mass calibration was performed using caffeine, MRFA, and Ultramark 1621 (Aldrich) in the mass-to-charge (m/z) range 195−1822 Da. All spectra were acquired within the m/z range of 150−2000 Da with a spray voltage of 4.5 kV, a capillary voltage of 44 V, a capillary temperature of 275 °C, and a flow rate of 3.00 μL/min.

Scheme 3. Examples of Chemical Structures Incorporated into the Structural Library[a]

Linear Chain 1

Ideal Star

AIBN Terminated Star 2

Star-Star Couple 1

Disproportionation Star 1a

Disproportionation Star 1b

[a] Such structures are associated with the conventional R-group approach RAFT star polymerization mechanistic scheme (when using MA as the monomer). Repeating monomer units have been enclosed with parentheses. Because of the high number of structures incorporated into the library, only a limited number of illustrative examples have been shown.
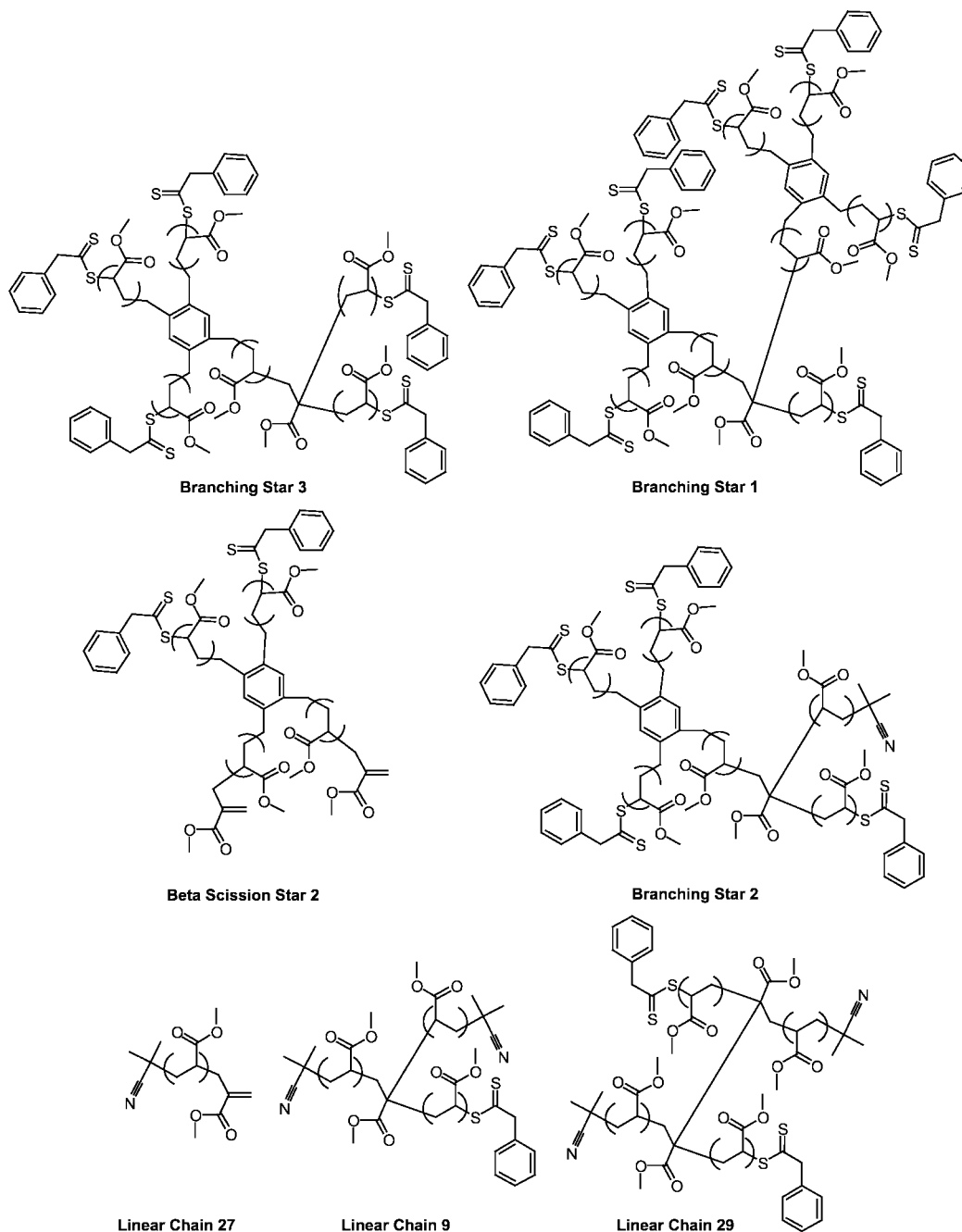
Nitrogen was used as sheath gas (flow: 50% of maximum), and helium was used as auxiliary gas (flow: 5% of maximum). Three microscans, with a maximum inject time of 100 ms per microscan, were averaged for each scan when using the normal scan type. When using the ZoomScan scan type, five microscans were averaged per scan, with a maximum inject time of 50 ms per microscan. Typical m/z value errors were observed to be ±0.3 Da.

Two-stage mass spectrometry (MS/MS) experiments were conducted upon precursor ions of interest in order to gain additional structural information from the resulting fragmentation patterns. All spectra were acquired using identical source conditions to the single-stage mass spectrometry experiments. A collision gas of helium was used at a partial pressure of 0.1 Pa, and typical normalized collision energies ranged from 25 to 30%.

Two different solvent mixtures were used during the preparation of samples for MS analysis: a 75/25 vol % mixture of dichloromethane (DCM)/methanol (MeOH) or a 60/40 vol % mixture of tetrahydrofuran (THF)/MeOH. In addition to solvent mixtures in which metal salts were not added, 60/40 vol % THF/MeOH mixtures doped with sodium iodide (0.1 mM), lithium iodide (0.3 mM), or potassium iodide (0.3 mM) were also used.

Results and Discussion

The polymerization conditions employed in the present study are discussed below, followed by a discussion of the structural library created for the R-group approach RAFT MA star polymer system under investigation. In-depth analyses of ESI-MS spectra generated from this system are then presented. Spectra obtained over various m/z ranges are discussed system-

Scheme 4. Examples of Chemical Structures Incorporated into the Structural Library[a]

Branching Star 3

Branching Star 1

Beta Scission Star 2

Branching Star 2

Linear Chain 27

Linear Chain 9

Linear Chain 29

[a] Such structures are potentially formed in R-group approach RAFT MA star polymerizations via the reaction pathways available to MCRs, as illustrated in Scheme 2. Repeating monomer units have been enclosed with parentheses. Because of the high number of structures incorporated into the library, only a limited number of illustrative examples have been shown.

atically, and the chemical structures assigned to these spectra are routinely summarized. Following this is a discussion of the insights gained from the ESI-MS investigations into the formation processes involved in living acrylate star polymerizations.

Polymerization Conditions. Given that high-accuracy data are only able to be obtained on the LCQ Deca ion trap instrument to a m/z of no more than 2000, there is a limit to the degree of polymerization (DP_n) of products able to be detected using this technique. For instance, given that the exact masses of the 4-arm RAFT agent employed in this study and an MA repeat unit are 798.07 and 86.04 Da, respectively, in such an MA system, singly charged sodiated adducts may only be directly observed for ideal star molecules with a DP_n of 13 or below and for star−star couples with a DP_n of 8 or below. Thus,

in order to be able to observe oligomeric/polymeric products of interest within this limited m/z window, the polymerization conditions employed in the preparation of the star polymer samples were carefully chosen. The chosen polymerization conditions sought to emphasize potential reaction pathways leading to nonideal star material and to allow the products generated via these reaction pathways to be observed within the 2000 m/z limit of the LCQ Deca ion trap instrument (see the Experimental Section for the specific polymerization conditions).

In order to achieve this, the acrylate monomer MA was chosen for its relatively low mass, which allows chains of a higher DP_n relative to other acrylates to be detected given the limited m/z range. Additionally, polymerization conditions were
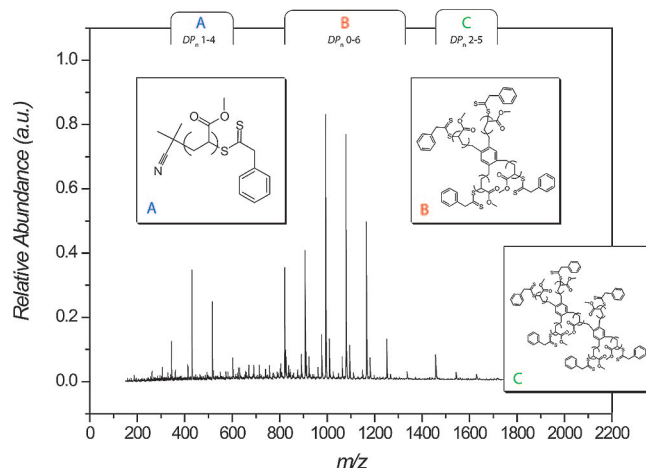
Figure 1. Typical ESI-MS spectrum obtained from an R-group approach RAFT MA star polymer sample using a normal scan type over the m/z range 150–2000. The m/z regions labeled A, B, and C are dominated by peaks arising from initiator fragment derived linear chains, ideal stars (along with the RAFT agent), and star–star couples, respectively.[62] These structures are illustrated in the boxes labeled A, B, and C, respectively (repeating monomer units have been enclosed with parentheses).

chosen to create a high radical flux, thereby placing an emphasis upon termination events and MCR formation. This was achieved by using a high initiator concentration, and the polymerizations were conducted with a cosolvent of toluene in order to decrease the rate of propagation, resulting in a higher number of transfer and termination events having occurred within the system at a given average DP_n. It was therefore also important to conduct the polymerizations at a temperature in which the rate of propagation remained relatively low; thus, polymerizations were conducted at 65 °C and not at a higher temperature. Since the incidence of β-scission reactions decrease as reaction temperatures decrease,[30] it is therefore unlikely that β-scission reactions are pronounced under the 65 °C polymerization temperature employed in the present study. These polymerization conditions aimed to create highly structured MWDs within the limited m/z range of the LCQ Deca ion trap instrument, and though the reaction pathways emphasized in the present study may not necessarily be prominent under all acrylate star polymerizations conditions, this does not negate the predominant aim of these experiments; that is, to allow reaction pathways that can potentially be of significance in acrylate star polymerizations to be unambiguously revealed.
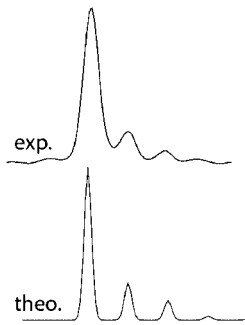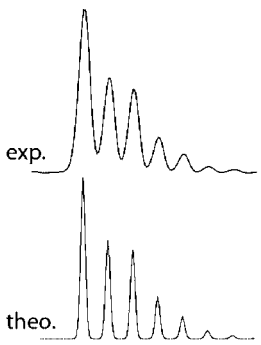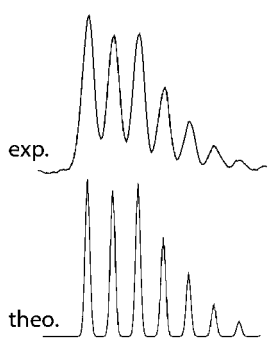
Structural Library. To assign chemical structures to the R-group approach RAFT MA star polymer system under investigation when using ESI-MS, comprehensive structural libraries containing products potentially generated during these polymerizations were created. Products likely to be formed in accordance with the conventional R-group approach RAFT star polymerization mechanistic scheme were incorporated into this library (see Scheme 3 for examples of these structures). These products include initiator fragment derived linear chains (e.g., Linear Chain 1 of Scheme 3), Ideal Star molecules (ideal star of Scheme 3), and closed-ring radical initiated and terminated stars (see Scheme S1 of the Supporting Information for illustrated examples of these structures) as well as all of the associated termination by combination (e.g., AIBN Terminated Star 2 of Scheme 3) and termination by disproportionation (e.g., Disproportionation Stars 1a and 1b of Scheme 3) products for these various species. In addition to these aforementioned products, chemical structures likely to be generated as a consequence of MCR formation on linear chains and star arms were also incorporated into the structural library (see Scheme 4 for examples of these structures). Products associated with β-scission (e.g., Linear Chain 27 and Beta Scission Star 2 of Scheme 4), termination by both disproportionation and combination (e.g., Linear Chains 9 and 29 and Branching Stars 1 and

2 of Scheme 4), and repropagation (e.g., Branching Star 3 of Scheme 4) of these MCRs were included. It should be noted that MCRs formed via intramolecular transfer reactions will produce short-chain branching products identical in mass to conventional nonbranched polymers if they take part in repropagation or coupling events. Such short-chain branching products are therefore unable to be distinguished from similar unbranched products when using MS. Finally, star and linear polymer chains containing thiol end groups,[53,57] thiolactone end groups and disulfide linkages,[57] in addition to cross-termination products[58] and oxidation products,[53,54] were also incorporated into the structural library.

For every compound incorporated into the structural library, the masses of adducts formed from these compounds via the attachment of various different species ($[P + (M)_n]^{n+}$, where P represents a star or linear polymer molecule; M represents a solvent molecule or sodium, potassium, lithium, silver, hydrogen, or ammonium cations; and $n = 1$ for singly charged ions or $n = 2$ for doubly charged ions) were calculated. The exact masses calculated for these adduct species are used in the assignment of peaks generated in the ESI-MS experiments. The masses of various salt cluster complexes ($[P + M(MX)_n]^{n+}$, where MX represents the metal salt and M the metal cation, and $n = 1$ or 2) were also calculated for use in the cases in which metal salts are added as dopants in the ESI-MS experiments.

Analyses of Spectra. By matching masses calculated from the structural library with the m/z of peaks observed in ESI-MS spectra generated from samples obtained from R-group approach RAFT MA star polymerizations, a detailed mapping of the chemical structures produced in these polymerizations is able to be conducted. An in-depth discussion of this process follows, focusing upon spectra produced over various ESI-MS m/z scan ranges. The discussion begins with an analysis of spectra produced using the normal scan type[59] of the LCQ Deca ion trap instrument over the m/z range 150–2000. Following this is an analysis of spectra produced using the ZoomScan scan type[60] over significantly smaller m/z ranges. When using the ZoomScan scan type, the signal-to-noise ratio observed in the generated spectrum is improved relative to that observed when using the normal scan mode. This increases the sensitivity of the analysis, allowing products to be detected which might otherwise have remained unobserved. Thus, the discussion of the spectra produced using the normal scan type over the m/z range 150–2000 is limited to the general features of the observed MWD, and detailed attempts at assigning structures to lower

Table 1. Ion Assignments for the Most Abundant Peaks Observed in Regions A, B, and C of the Spectrum Depicted in Figure1

m/z region	ion assignment for dominant peaks	DP_n[63]	$m/z_{exp.}$	$m/z_{theo.}$	error (*m/z*)	simulated/experimental isotopic peak patterns[64]
A	[Linear Chain 1 + Na]$^+$	1-5	430.3	430.1	0.2	exp. / theo.
B	[Ideal Star + Na]$^+$	1-7	993.1	993.1	0.0	exp. / theo.
C	[Star-Star Couple 1 + Na]$^+$	1-5	1457.0	1457.2	0.2	exp. / theo.

abundance peaks are only conducted upon the ZoomScan spectra. These ZoomScans were obtained over representative areas of the full scan range and encompass all of the peaks of interest observed within this *m/z* range.

It should also be noted that when dealing with products that form ions that are detected at levels only marginally above acceptable signal-to-noise ratios, as is the case in the present study, particular care must be taken to ensure that the peaks to which structures are assigned genuinely arise as a result of products of interest (i.e., products generated via significant reaction pathways in R-group approach RAFT MA star polymerizations). Thus, for a single polymer sample, multiple solutions were prepared for ESI-MS analysis to test for reproducibility. As an additional test for reproducibility, different polymer samples produced using identical reaction conditions were analyzed using ESI-MS. From these spectra, peaks are confidently assumed to arise from products of interest if they (a) are consistently reproducible in all of the spectra obtained and (b) reoccur at a *m/z* 86.04 higher than the original peak (i.e., a mass corresponding to a product peak that is exactly one monomer repeat unit larger than the original peak),[61]

suggesting that such peaks are indeed due to oligomeric/polymeric chains and not impurities within the sample. In the following analyses, peaks marked with an "x" are not able to be confidently identified as oligomer/polymer product peaks of interest, either because they are not reproducible or because they are not periodic.

Normal Scan Type Spectra Obtained over the Range 150–2000 m/z. Figure 1 shows a typical ESI-MS spectrum obtained from an R-group approach RAFT MA star polymer sample using a normal scan type over the *m/z* range 150–2000. A highly structured MWD is observed, indicating that reaction pathways leading to nonideal star material play a significant role in the polymerization system under investigation. Indeed, the dominant peaks in the *m/z* regions labeled as A, B, and C in Figure 1 can be assigned to initiator-derived linear chains, ideal stars, and star–star couples, respectively (see Table 1).

These assignments are in excellent agreement with the conclusions gathered from previous studies on R-group approach RAFT star polymerizations,[19,20] which suggested that initiator-derived linear chains and star–star couples are the predominant nonideal star contributors to the highly structured MWDs which

Scheme 5. Fragmentation Pathways Observed in MS/MS Experiments Conducted upon Oxidized Star Molecules[a]

168.0 Da

184.0 Da

152.0 Da

X Denotes a Star Couple
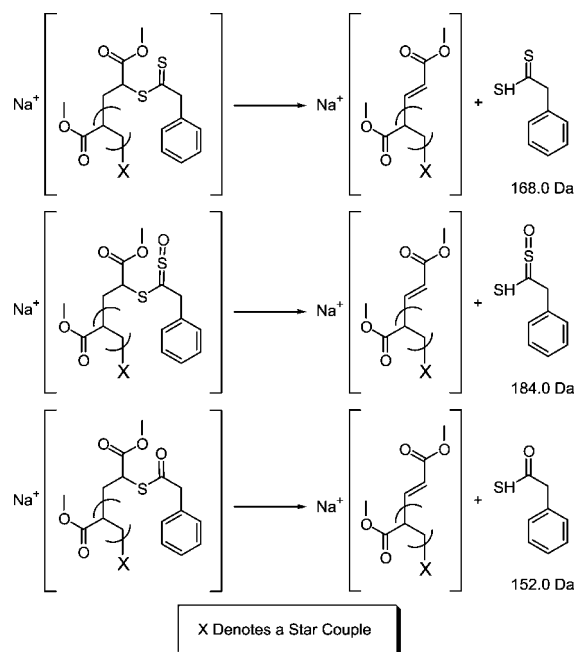
[a] Precursor and daughter ions are detected as sodium adducts.
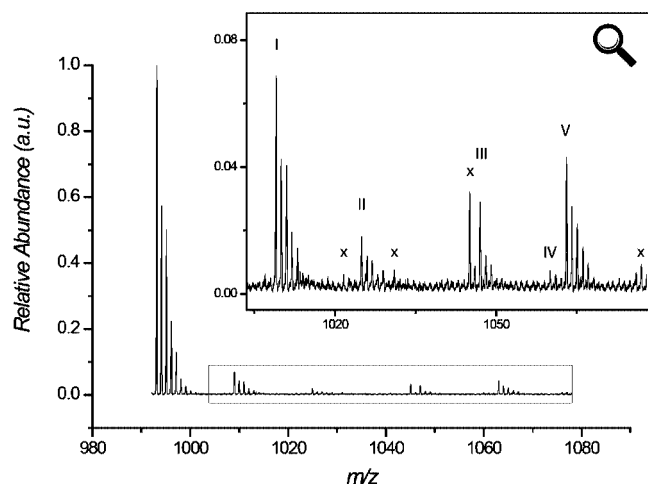

Figure 2. Typical ZoomScan spectrum obtained from the ideal star dominated *m/z* region of the full scan range (region B of Figure 1). The inset shows a magnified view of the spectrum, with peak labels. Peaks labeled "x" are either nonreproducible or nonperiodic.

Table 2. Potential Ion Assignments for Peaks I, II, III, and V of Figure 2 Based on Matching Experimentally Observed and Theoretical Mass-to-Charge Ratios

peak label	possible ion assignments	m/z_{exp}	m/z_{theo}	error (m/z)
I	[oxidized ideal star 1 + Na]⁺	1009.0	1009.1	0.1
	[ideal star 1 + K]⁺		1009.1	0.1
II	[oxidized ideal star 2 + Na]⁺	1025.0	1025.1	0.1
	[oxidized ideal star 1 + K]⁺		1025.1	0.1
	[branching star 26 + Na]⁺		1025.1	0.1
III	[oxidized ideal star 6 + Na]⁺	1047.0	1047.2	0.2
	[oxidized ideal star 5 + Li]⁺		1047.2	0.2
	[branching star 27 + Li]⁺		1047.2	0.2
V	[oxidized ideal star 5 + Na]⁺	1063.1	1063.2	0.1
	[ideal star 1 + Li]⁺		1063.2	0.1
	[branching star 27 + Na]⁺		1063.2	0.1

can be observed in such systems. In addition to these peaks, a host of lower abundance product peaks are observed in the spectrum. Higher resolution spectra were taken in order to image

Table 3. Mass Losses Observed in MS/MS Experiments Conducted upon Peaks I, II, III and V, As Labeled in Figure2
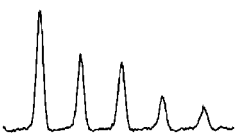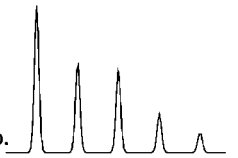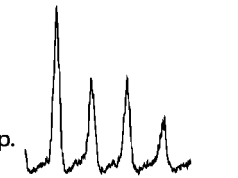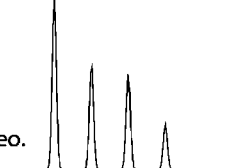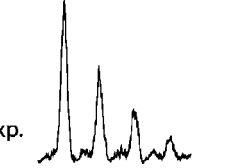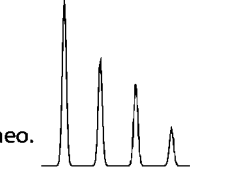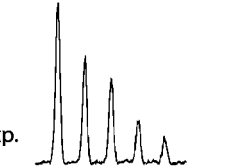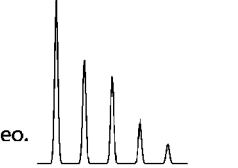
peak label	oxidation product ion assignment	168.0 Da	184.0 Da	152.0 Da	theoretically expected mass losses
I	[oxidized ideal star 1 + Na]⁺	Y	Y	N	168.0 and 184.0
II	[oxidized ideal star 2 + Na]⁺	Y	Y	N	168.0 and 184.0
III	[oxidized ideal star 6 + Na]⁺	Y	N	Y	168.0 and 152.0
V	[oxidized ideal star 5 + Na]⁺	Y	N	Y	168.0 and 152.0

the ions that produce these peaks with a heightened degree of accuracy and sensitivity, and the analyses of these spectra are presented below.

ZoomScan Spectra Obtained over the Ideal Star-Dominated m/z Region. ZoomScan spectra were taken over representative *m/z* areas of the region dominated by ideal star peaks (labeled region B in Figure 1), and Figures 2 and S1 show typical examples of such spectra. A significant number of nonreproducible and/or nonperiodic peaks are observed in these spectra, which is not unexpected given that low abundance peaks are being analyzed. As stated in the introduction to the analyses of the spectra, only consistently reproducible, periodic peaks are deemed to arise from products of interest; hence, only such peaks are assigned to products in the following discussion.

Within the ideal star-dominated region in question, six additional peaks corresponding to products of interest are able to be identified (peak VI appears for the first time at *m/z* 1158.9 and is therefore not shown in Figure 2; a depiction of peak VI is found in Figure S1 of the Supporting Information). By comparing theoretical *m/z* values to these peaks, matches with adduct species are able to be obtained. Only some of the products which can give rise to such adduct species are mechanistically feasible; thus, the mechanistically unrealistic assignments are disregarded. For example, the experimentally observed *m/z* of peak I matches with the theoretical *m/z* of sodium adducts formed from the products Disproportionation Stars 3b and 4e, star products in which 3 or 4 star arms have been terminated via disproportionation reactions. If disproportionation reactions were indeed occurring upon 3 or 4 star arms, peaks resulting from products in which 2 arms have been

Table 4. Ion Assignments for the Product Peaks Labeled in the Spectra Depicted in Figures 2 and S1[a]

Peak Label	ion assignment	DP_n^{63}	$m/z_{exp.}$	$m/z_{theo.}$	error (m/z)	simulated/experimental isotopic peak patterns[64]
I	[Oxidized Ideal Star 1 + Na]$^+$	1-6	1009.0	1009.1	0.1	exp. / theo.
II	[Oxidized Ideal Star 2 + Na]$^+$	1-5	1025.0	1025.1	0.1	exp. / theo.
III	[Oxidized Ideal Star 6 + Na]$^+$	1-4	1047.0	1047.2	0.2	exp. / theo.
IV	[Branching Star 2 + Na]$^+$	2-4	1060.0	1060.2	0.2	low signal-to-noise; see Table S2
V	[Oxidized Ideal Star 5 + Na]$^+$	1-5	1063.1	1063.2	0.1	exp. / theo.
VI	[Branching Star 3 + Na]$^+$	2-4	1158.9	1159.1	0.2	low signal-to-noise; see Table S2

[a] Where product peaks have been depicted more than once, mass-to-charge ratios and isotopic peak patterns have been given for the most abundant product peak. The experimental isotopic peak patterns for the ion assignments labeled as "low signal-to-noise" are subject to significant distortion from experimental noise. The simulated and experimental isotopic peak patterns for these ions are depicted in Table S2 of the Supporting Information.
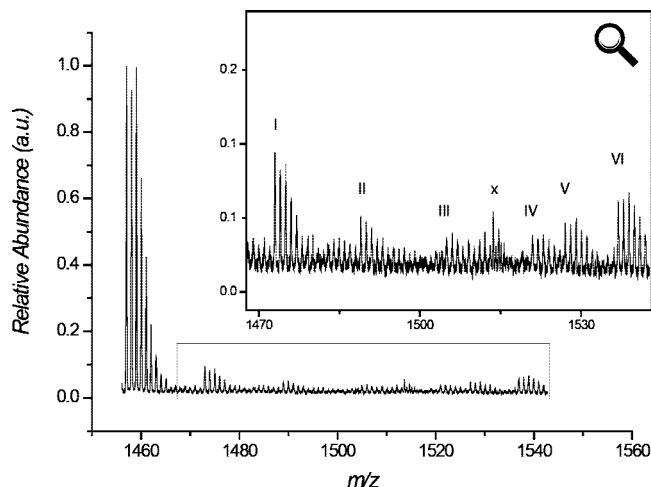
Figure 3. Typical ZoomScan spectrum obtained from the star–star couple dominated *m/z* region of the full scan range (region C of Figure 1). The inset shows a magnified view of the spectrum, with peak labels. The peak labeled "x" is nonreproducible and nonperiodic.

terminated via disproportionation reactions would also be expected to arise. As no peaks corresponding to disproportionation products involving 2 star arms are observed within the full 150–2000 *m/z* scan range, adducts formed from the Disproportionation Stars 3b and 4e products are disregarded as potential peak assignments.

After disregarding such mechanistically unfeasible assignments, peaks IV and VI can be confidently assigned to single products, whereas peaks I, II, III, and V are still able to be assigned to multiple adduct species (as summarized in Table 2). For example, all of these peaks may be assigned to sodium adducts formed from oxidation products. Specifically, peaks I and II are able to be assigned to oxidation products in which an oxygen atom attaches to the RAFT end group on one or two star arms, respectively, and peaks III and V are able to be assigned to oxidation products in which a sulfur atom is replaced with an oxygen atom on the RAFT end group of one- or two-star arm, respectively (see Scheme S2 of the Supporting Information for illustrations). The low abundances of peaks II and III relative to peaks I and V support these product assignments. This is because oxidation reactions involving a maximum of only two star arms are potentially observed, which indicates that if oxidation reactions do indeed take place, the extent to which such reactions occur is limited. Hence, fewer star products would be expected to be formed from oxidation reactions involving two star arms relative to reactions involving only one star arm.

In addition to the aforementioned potential assignments, peaks II and V may also be matched with sodium adducts arising from thiol-terminated products, which are potentially formed from the degradation of one or two RAFT end groups of the Branching Star 3 parent species (Branching Stars 26 and 27 respectively; see Scheme S3 of Supporting Information for illustrations of these structures). These assignments are mechanistically feasible, as the Branching Star 3 product is able to be identified (assigned to peak VI, Figure S1). Finally, peaks I, II, III, and V may also be assigned to potassium and lithium adducts of ideal stars (peaks I and V) or of the aforementioned oxidation or thiol-terminated products (peaks II and III). Thus, it can be seen that there is a significant degree of ambiguity in the assignment of products to peaks I, II, III, and V.
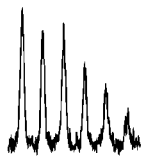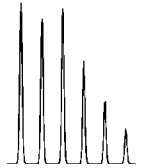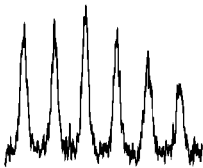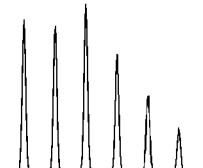
When considering, among other pieces of evidence, the abundances of peaks I, II, III, and V, it would at first appear that the oxidation product assignments are the most probable and that the other assignments are less sound. (A detailed discussion outlining the reasoning behind these conclusions may

be found in the Supporting Information.) However, the presence of these peaks arising as a consequence of oxidation products being present in the sample solutions is still questionable. This is because the formation of such oxidation products have previously been explained by the presence of peroxides in the THF used to prepare samples for ESI-MS analysis,[52–54] and the abundances of such oxidation product peaks are known to fluctuate between spectra produced from otherwise identical samples, most probably due to different degrees of oxidation taking place in samples that are stored over different lengths of times.[51] However, in the present study, the relative abundances of the peaks assigned to oxidation products remain relatively consistent between different spectra, and more importantly, these peaks are observed whether or not THF is used as the solvent. Thus, adducts formed from oxidation products generated as a result of the presence of peroxides in THF are not an adequate explanation for the ambiguous peaks in question. As other similar product peaks are observed throughout spectra taken across the full available *m/z* range and as the correct assignments for these peaks can be vital when making inferences with regards to the formation pathways involved in the acrylate system under investigation, it was deemed necessary to conduct further experiments to thoroughly test the potential peak assignments in order to unambiguously identify the origins of these peaks.

First, to test the potential contribution of lithium and/or potassium adduct formation in the generation of these ambiguous peaks, samples were prepared using solvents doped with sodium iodide, lithium iodide, or potassium iodide, and ZoomScan spectra were obtained from these samples over the *m/z* region 940–1050 (spectra obtained from the potassium and lithium cation doped samples are shown in Figure S2). By introducing a significant quantity of a single type of metal ion into the sample solutions, adducts formed between these particular cations and products present in the sample solution would be expected to be prominent. By comparing the relative abundance of the peaks observed in spectra produced from the differently doped samples, it is possible to draw conclusions relating to the contribution of certain metal adducts toward peaks of a given *m/z*. These experiments strongly suggested that the ambiguous product peaks labeled I, II, III, and V in Figure 2 arise predominantly, if not entirely, from sodium adducts formed from either oxidation products or from thiol-terminated chains and have been detailed in full in the Supporting Information.

Having confidently ruled out potassium and lithium adducts as significant contributors to the ambiguously assigned product peaks, further tests were undertaken upon freshly prepared ESI-MS samples and samples left in storage (discussed in full in the Supporting Information). These experiments showed that oxidation of RAFT end groups does indeed occurs readily in THF/MeOH solutions, but only to a minor extent in DCM/MeOH solutions, indicating that peaks I, II, III, and V of Figure 2 either are due to oxidation products that form prior to preparation of the sample solution or are due to other product species altogether. In order to test this, MS/MS spectra were generated from suspected oxidation product peaks in a typical R-group approach RAFT MA star polymer sample and from known oxidation product peaks in heavily oxidized THF/MeOH samples. Fragment ions associated with mass losses of 168.0, 184.0, and 152.0 Da are observed in the MS/MS spectra produced from product peaks associated with oxidized stars in the THF/MeOH sample. These are in accordance with fragmentation pathways associated with star arms carrying a RAFT end group or one of two forms of the oxidized RAFT end group, resulting in the loss of the respective RAFT end group from the molecular ion, leaving behind a star molecule carrying an unsaturated arm (as illustrated in Scheme 5). Importantly, the

Table 5. Ion Assignments for the Product Peaks Labeled in the Spectrum Depicted in Figure 3[a]

Peak Label	ion assignment	DP_n[63]	$m/z_{exp.}$	$m/z_{theo.}$	error (*m/z*)	simulated/experimental isotopic peak patterns[64]
I	[Oxidized Star-Star Couple 1 + Na]$^+$	2-4	1473.0	1473.2	0.2	
II	[Oxidized Star-Star Couple 2 + Na]$^+$	2-3	1489.0	1489.2	0.2	low signal-to-noise; see Table S3
III	[Oxidized Star-Star Couple 3 + Na]$^+$	2-3	1504.9	1505.2	0.3	low signal-to-noise; see Table S3
IV	[Oxidized Star-Star Couple 4 + Na]$^+$	2-3	1521.0	1521.2	0.2	low signal-to-noise; see Table S3
V	[Oxidized Star-Star Couple 7 + Na]$^+$	2-4	1527.1	1527.0	0.1	low signal-to-noise; see Table S3
VI	[Branching Star 1 + Na]$^+$	1-3	1537.0	1537.2	0.2	

[a] The experimental isotopic peak patterns for the ion assignments labeled as "low signal-to-noise" are subject to significant distortion from experimental noise. The simulated and experimental isotopic peak patterns for these ions are depicted in Table S3 of the Supporting Information.

mass losses observed in the MS/MS spectra generated from peaks I, II, III, and V show perfect agreement with the expected oxidized RAFT groups corresponding to these peaks, as illustrated in Table 3. This confirms that peaks I, II, III, and V can be assigned to sodium adducts formed from oxidized star species.

From the above experiments, it can be concluded that peaks I, II, III, and V can be assigned predominantly, if not entirely, to sodium adducts formed from oxidized star molecules and that these oxidized products are formed prior to preparation of the solutions used in the ESI-MS analyses. The relatively high abundance of these products suggests that the oxidation reactions are occurring to a significant extent through storage of the polymer samples, which had been exposed to the atmosphere. It is suggested that the presence of residual AIBN in the polymer samples may act as an initiator for these oxidation reactions,[65–67] explaining the high degree to which the oxidation products are formed. By establishing that these previously ambiguous peaks are indeed due to sodium adducts formed from oxidation products, peaks in which similar ambiguities in product assignments are encountered are immediately assigned to oxidation products in the analyses of the subsequent ZoomScan spectra obtained over different *m/z* regions.

The final assignments for all of the product peaks of interest in the ideal star-dominated *m/z* region are summarized in Table 4. It should be noted that the experimentally observed isotopic peak patterns for several of the product peaks of interest are potentially subject to significant distortion due to the particularly low signal-to-noise ratios of these peaks (such peaks have been depicted in Table S2 of the Supporting Information). After taking these potential distortions into account, the general patterns in the isotope abundances for these product assignments are favorably comparable to the simulated isotopic peak patterns.

ZoomScan Spectra Obtained over the Star–Star Couple-Dominated m/z Region. A typical ZoomScan spectrum taken over a representative *m/z* area of the region dominated by star–star couple peaks (labeled region C in Figure 1) is shown in Figure 3. As per the previously discussed spectra, only consistently reproducible, periodic peaks are assigned to products.

A summary of the ion assignments for product peaks of interest observed in spectra obtained over the star–star couple
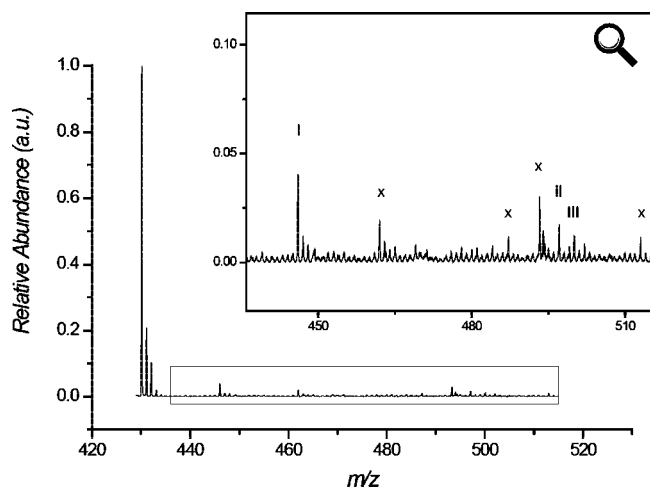
Figure 4. Typical ZoomScan spectrum obtained from the linear chains dominated *m/z* region of the full scan range (region A of Figure 1). The inset shows a magnified view of the spectrum, with peak labels. Peaks labeled "x" are either nonreproducible or nonperiodic.
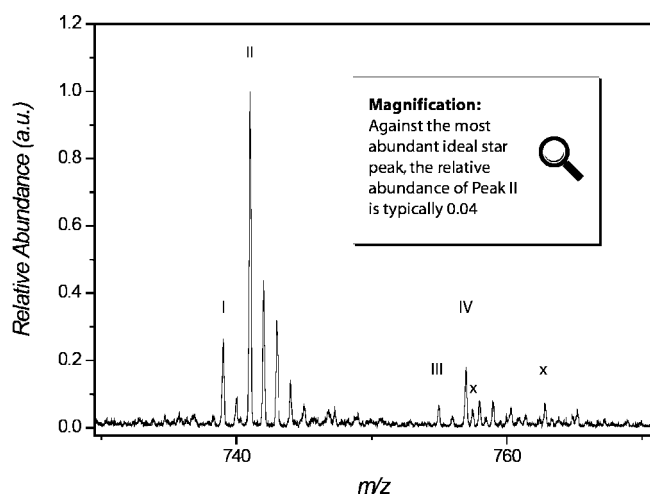

Figure 5. Typical ZoomScan spectrum obtained in the *m/z* range 730–770, with peak labels. Peaks labeled "x" are either nonreproducible or nonperiodic.

dominated *m/z* region is given in Table 5. It can be seen that, once again, a significant number of peaks associated with oxidation are observed. Additionally, a long-chain branching product formed as a result of the termination of a propagating star, or a radical carrying star core, with an intermolecularly formed MCR on a star arm is assigned to peak VI. Because of the low signal-to-noise ratios of the product peaks of interest within this *m/z* region, the experimentally observed isotopic peak patterns for a significant number of these peaks are subject to considerable distortion. However, as with previously described product assignments, the general isotope distributions in the simulated and experimentally observed isotopic peak patterns compare favorably after this potential distortion is taken into account (see Table S3). Particularly noteworthy is the simulated isotopic peak pattern for the ion assignment of peak VI. This assignment corresponds to a MCR-derived long-chain branching product with seven RAFT end groups, which represents one more RAFT end group than a conventional star–star couple. The additional RAFT end group significantly increases the abundance of the third isotope peak due to the existence of the extra two sulfur atoms, differentiating the expected isotopic peak pattern from conventional star–star couples and their oxidation products. This difference is indeed observed experimentally,

providing a strong affirmation of the veracity of the product assignment.

ZoomScan Spectra Obtained over the Linear Chains-Dominated m/z Region. A typical ZoomScan spectrum taken over a representative *m/z* area of the region dominated by linear chain peaks (labeled region A in Figure 1) is shown in Figure 4. Once again, only consistently reproducible, periodic peaks are assigned to products.

A summary of the ion assignments for product peaks of interest observed in spectra obtained over this region is given in Table 6. Oxidation products are again apparent, and an additional product formed as a result of a termination pathway involving an intermolecularly formed MCR on a linear chain is assigned to peak II. It should be noted that the experimentally observed isotopic peak patterns for peaks II and III overlap, and the isotopic peak pattern simulations have been created to reflect this. Thus, there is a certain degree of artificiality in the similarities observed between the experimental and simulated patterns, as the abundance of the first isotope peak of the simulated pattern of peak III was scaled to reflect the experimentally observed abundance relative to peak II. However, after taking this into account, the favorable comparison between the two patterns is still legitimate after considering distortions from experimental noise.

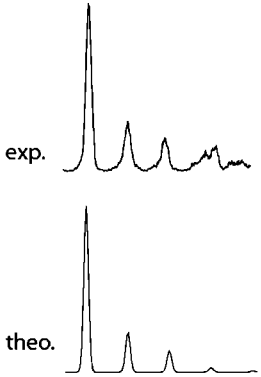*ZoomScan Spectra Obtained over Additional m/z Regions.* In addition to the peaks which have already been listed, product peaks of interest are also able to be identified in *m/z* ranges that lie outside of the regions dominated by linear chain, ideal star, and star–star couples. These product peaks are presented below.

A typical ZoomScan spectrum obtained in the *m/z* range 730–770 is presented in Figure 5. The peak assignments for the product peaks of interest in this *m/z* range are presented in Table 7, along with ion assignments for peaks which have not been labeled in illustrated spectra. The spectra encompassing these latter peaks are not presented because the majority of the peaks within the *m/z* region in which they lie correspond to lower abundance peaks which have already been depicted and assigned. In addition to further oxidation products, stars with single arms terminated via disproportionation reactions are also identified, along with stars in which single arms have been terminated via combination with an AIBN fragment or an AIBN fragment derived linear chain. The saturated star disproportionation product may also be formed via transfer reactions (this is elaborated upon in the Summary of the Structural Assignments and their Mechanistic Implications section).

The experimentally observed isotopic peak patterns for peaks I and II, peaks III and IV, and the peaks assigned to the [Oxidized RAFT Agent 5 + Na]+ and [AIBN Terminated Star 1+ Na]+ adducts overlap. As discussed previously, the attempts at simulating isotopic peak patterns to reflect this signal overlap create a certain degree of added comparability between the simulated and experimentally observed isotope distributions. However, even after this is considered, the favorable comparisons between the two distributions are once again still legitimate for all of the ion assignments after experimental noise has been taken into account.

Summary of the Structural Assignments and Their Mechanistic Implications. A summary of all of the nonoxidized products identified in the R-group approach RAFT MA star polymer system under investigation within the full *m/z* range of the LCQ Deca ion trap instrument is presented in Table 8, along with a summary of the formation processes involved in the generation of these products (for illustrated examples of oxidized products, see Scheme S2 of the Supporting Information). These final product assignments are listed in order of decreasing relative abundance, as observed for the most

Table 6. Ion Assignments for the Product Peaks Labeled in the Spectrum Depicted in Figure4[a]

Peak Label	ion assignment	DP_n[63]	$m/z_{exp.}$	$m/z_{theo.}$	error (m/z)	simulated/experimental isotopic peak patterns[64]
I	[Oxidized Linear Chain 1 + Na]$^+$	1-3	446.0	446.1	0.1	exp. theo.
II	[Linear Chain 9 + Na]$^+$	1-4	497.1	497.2	0.1	low signal-to-noise; see Table S4
III	[Oxidized Linear Chain 2 + Na]$^+$	2-3	500.1	500.2	0.1	low signal-to-noise; see Table S4

[a] The experimental isotopic peak patterns for the ion assignments labeled as "low signal-to-noise" are subject to significant distortion from experimental noise. The simulated and experimental isotopic peak patterns for these ions are depicted in Table S4 of the Supporting Information.

abundant peak to which each product was assigned in a typical normal scan type spectrum obtained over the m/z range 150–2000.[68] Though these relative abundances provide some indication of the propensity for certain products to be formed in the star acrylate system under study, and hence of the kinetic favorability of certain reaction pathways, such inferences must be made with caution due to the potential for mass bias effects and the potential for ionization bias effects stemming from differing end-group functionalization and/or the polarity of the polymer. For example, when considering relative abundances alone, it is difficult to conclude that the formation of star–star couples is favorable when compared to the formation of disproportionation products when two radical carrying star arms meet. This is particularly true for species which differ significantly in terms of their chemical constituents, as the potential for ionization bias effects is thereby heightened.
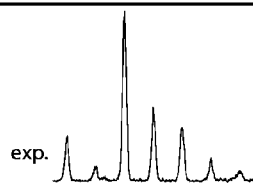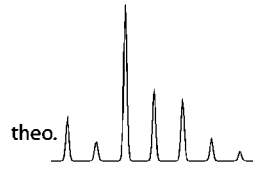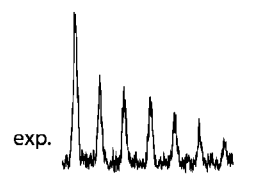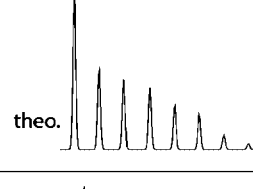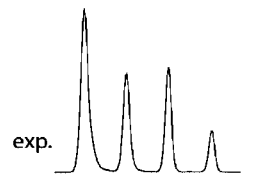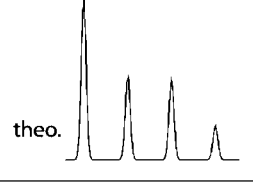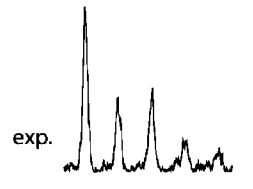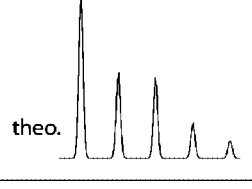
However, despite these difficulties in ascertaining the precise favorability of certain formation pathways from these studies, significant conclusions can be made with regards to the nature of the formation pathways which operate in R-group approach acrylate star polymerizations. In addition to ideal stars, it can be seen that the initiator derived linear chains and star–star couples are detected in significant abundances, providing further evidence to support the notion that the formation of these species are responsible for the highly structured MWDs capable of being produced in R-group approach star polymerizations. Other reaction pathways associated with the conventional R-group approach polymerization mechanistic scheme which are observed to be of importance are termination of star arms with initiator fragments or initiator derived linear chains and termination of star arms via disproportionation reactions. These termination reactions are observed to occur from a DP_n of one onward, indicating that such reactions can take place in close proximity to the star core. It is particularly noteworthy that the saturated star disproportionation product is significantly more abundant than the unsaturated disproportionation product (see Figure 5), as this unsaturated disproportionation product may also form via intermolecular transfer reactions in which a hydrogen atom is abstracted from a CTA. Given the high degree of chemical similarity between the two disproportionation products, ionization bias effects stemming from differing

chemical functionalization are unlikely to be significant. Additionally, the potential for mass bias effects may be disregarded, as the two products differ in mass by only ∼2 Da. Thus, it can be concluded with some degree of confidence that intermolecular transfer reactions are up to twice as likely to occur as disproportionation reactions.

As saturated linear chains are not observed whereas stars containing saturated arms are, it would appear that in the system under study intermolecular MCR formation expectedly occurs predominantly as a result of reactions involving radical carrying star products and not linear chains. However, it is the fate of such intermolecularly formed MCRs that is of particular interest to this study. The products assigned to the ESI-MS spectra indicate that these MCRs can terminate with initiator fragments, initiator derived linear chains, propagating stars, or radical carrying star cores and that these reactions can occur on MCRs formed on star arms or on linear chains. The MCR termination reactions involving propagating stars or radical carrying star cores are observed to occur from a DP_n as low as one, indicating that MCRs can form on products carrying only a single monomer unit. For MCR termination reactions involving initiator fragments or initiator derived linear chains, products with DP_ns as low as two are observed, once again indicating that MCR formation can occur on products carrying very few monomer repeat units. Repropagation of MCRs on star arms formed via intermolecular reactions is also observed to occur, and such reactions are also found to occur from a DP_n as low as two.

At the polymerization temperature of 65 °C employed in the present study, β-scission reactions were not observed, but it would be expected that such reactions can play a larger role in acrylate star polymerizations conducted at higher temperatures. Additionally, as branching products associated with intramolecular transfer reactions are unable to be observed when using ESI-MS, the reaction pathways leading to the formation of such products were unable to be distinguished in the present study. This does not rule out the likelihood of termination and propagation reactions occurring upon such MCRs in a manner similar to the pathways observed to occur on intermolecularly formed MCRs; however, because of the backbiting processes which must take place in order to form a MCR via an

Table 7. Ion Assignments for the Product Peaks Labeled in the Spectrum Depicted in Figure 5 and for Product Peaks Observed in ZoomScans Which Have Not Been Depicted[a]

Peak Label	ion assignment	$DP_n{}^{63}$	$m/z_{exp.}$	$m/z_{theo.}$	error (m/z)	simulated/experimental isotopic peak patterns[64]
I	[Disproportionation Star 1b + Na]$^+$	1-3	739.0	739.1	0.1	exp.
II	[Disproportionation Star 1a + Na]$^+$	1-3	741.0	741.1	0.1	theo.
III	[Oxidized Disproportionation Star 1b (1) + Na]$^-$	1-2	755.0	755.1	0.1	low signal-to-noise; see Table S5
IV	[Oxidized Disproportionation Star 1a (1)+ Na]$^-$	1-3	757.0	757.1	0.1	low signal-to-noise; see Table S5
n/a	[Oxidized RAFT Agent 5 + Na]$^+$	n/a	805.0	805.1	0.1	exp.
n/a	[AIBN Terminated Star 1+ Na]$^+$	1-2	808.2	808.1	0.1	theo.
n/a	[RAFT Agent + Na]$^+$	n/a	821.0	821.1	0.1	exp. / theo.
n/a	[Oxidized RAFT Agent 1 + Na]$^+$	n/a	837.0	837.1	0.1	exp. / theo.

[a] The experimental isotopic peak patterns for the ion assignments labeled as "low signal-to-noise" are subject to significant distortion from experimental noise. The simulated and experimental isotopic peak patterns for these ions are depicted in Table S5 of the Supporting Information.

Table 8. Summary of the Nonoxidized Products Observed in Spectra Produced from the R-Group Approach RAFT MA Star Polymerizations and the Formation Pathways under Operation in the Generation of These Products[69] [a]
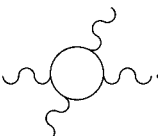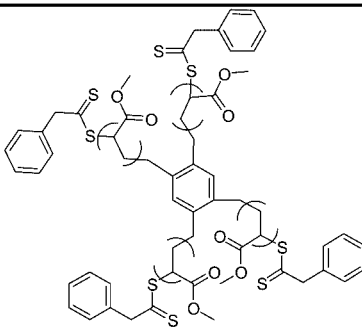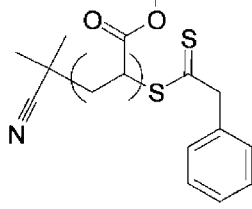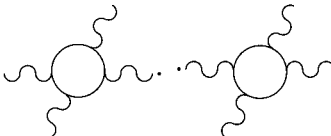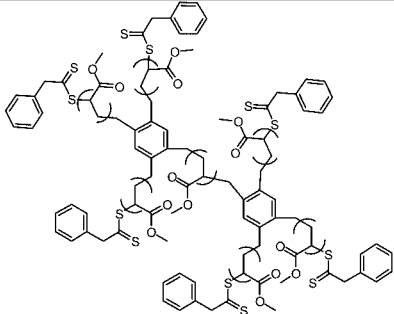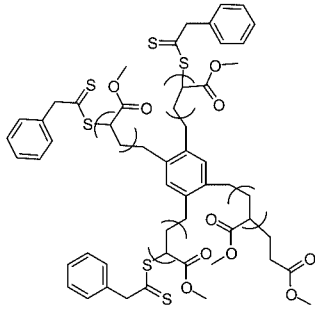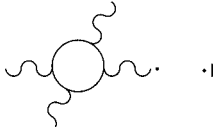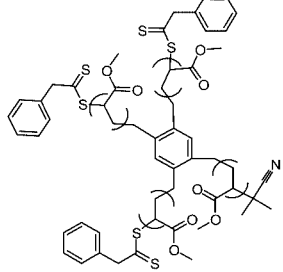
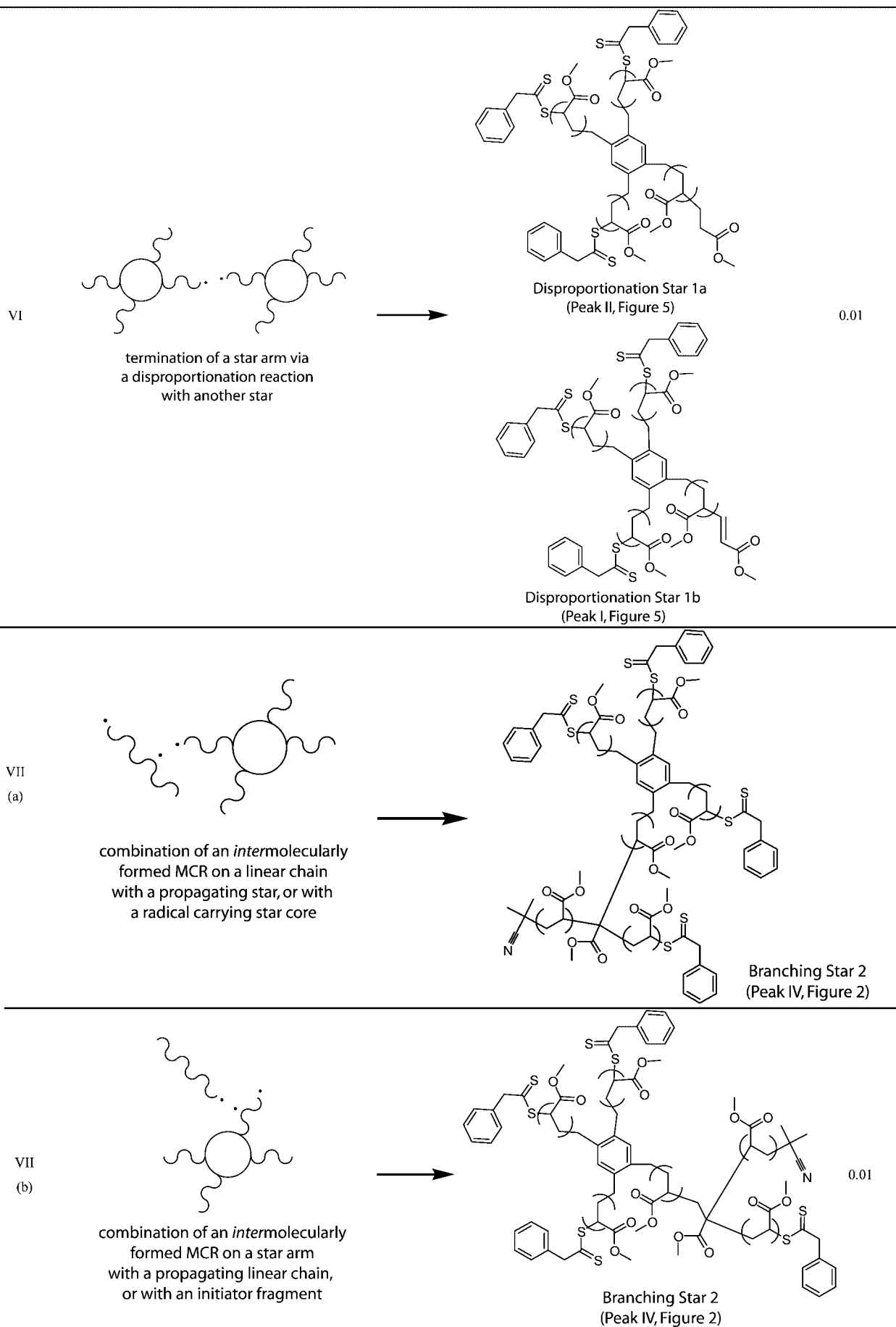| Formation Pathway	Product	Product Abundance
I propagation on star core (R-group initiation)	Ideal Star (Region *B*, Figure 1)	1.00
II propagation on linear chain (AIBN fragment initiation)	Linear Chain 1 (Region *A*, Figure 1)	0.35
III combination of 2 propagating stars, or a propagating star and a radical carrying star core	Star-Star Couple 1 (Region *C*, Figure 1)	0.09
IV *inter*molecular transfer of a star radical to a CTA	Disproportionation Star 1a (Peak II, Figure 5)	0.03
V combination of a star arm with an initiator fragment, or with a propagating linear chain	AIBN Terminated Star 1 (unlabeled peak, Table 7)	0.02

Table 8 Continued

VI

termination of a star arm via
a disproportionation reaction
with another star

Disproportionation Star 1a
(Peak II, Figure 5)

Disproportionation Star 1b
(Peak I, Figure 5)

0.01

VII
(a)

combination of an *inter*molecularly
formed MCR on a linear chain
with a propagating star, or with
a radical carrying star core

Branching Star 2
(Peak IV, Figure 2)

VII
(b)

combination of an *inter*molecularly
formed MCR on a star arm
with a propagating linear chain,
or with an initiator fragment

Branching Star 2
(Peak IV, Figure 2)

0.01

Table 8 Continued

VIII

re-propagation of an
*inter*molecularly formed
MCR on a star arm

Branching Star 3
(Peak VI, Figure S1)

0.01

IX

combination of an *inter*molecularly
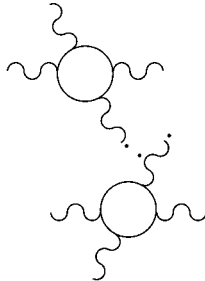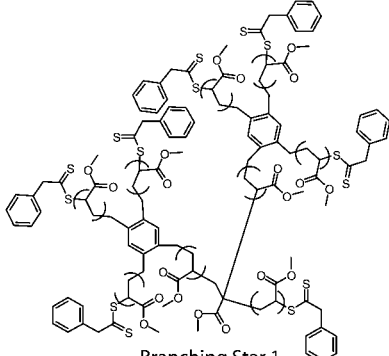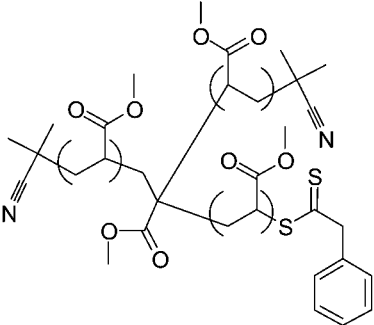formed MCR on a star arm
with a propagating star, or with
a radical carrying star core

Branching Star 1
(Peak VI, Figure 3))

0.01

X

combination of an *inter*molecularly
formed MCR on a linear chain
with a another linear chain, or with
an initiator fragment

Linear Chain 9
(Peak II, Figure 4)

0.01

[a] The products and their associated formation pathways are listed in order of the relative abundances of the most abundant peak to which each product was assigned in a typical normal scan type spectrum obtained over the *m/z* range 150–2000.

intramolecular reaction, it is unlikely that such processes occur at DP_ns as low as those observed for MCRs formed via intramolecular transfer reactions.

Conclusion

ESI-MS methodologies were successfully applied to map the product species generated in R-group approach RAFT MA star polymerizations, allowing insights to be gained into the formation processes under operation in living acrylate star polymerizations. Products associated with the conventional R-group approach RAFT star polymerization mechanistic scheme were observed; these products being initiator fragment derived linear chains, ideal stars, star–star couples, and terminated star products formed as a result of disproportionation and combination reactions. Importantly, products formed via reaction pathways involving MCRs were also imaged. These products were formed as a result of termination reactions involving intermolecularly formed MCRs on both star arms and linear chains with propagating stars, radical carrying star cores, AIBN

fragments, or AIBN derived linear chains. Additionally, products formed from the repropagation of intermolecularly formed MCRs on star arms were observed. The products formed from MCR derived reaction pathways were imaged from a DP_n as low as one, indicating that MCRs form on products carrying a single monomer unit.

Significant oxidation of RAFT end groups prior to preparation of the ESI-MS samples was observed. The extent of this oxidation was explained by the presence of residual AIBN in the polymer samples, which was hypothesized to act as an initiator for these oxidation reactions.

No β-scission reactions were observed at the polymerization temperature of 65 °C employed in the ESI-MS studies, and short-chain branching formation processes were unable to be imaged when using ESI-MS; however, these were not ruled out as potentially important reaction pathways in acrylate star polymerizations.

Supporting Information Available: Illustrations of closed-ring initiated star polymers, oxidation products, and thiol-terminated chains; additional spectrum generated within the ideal star dominated *m/z* region; a presentation of experimental data confirming the existence of oxidation products; and simulated/experimental isotopic peak patterns for peaks of low signal-to-noise. This material is available free of charge via the Internet at http://pubs.acs.org.

References and Notes

(1) Barner, L.; Davis, T. P.; Stenzel, M. H.; Barner-Kowollik, C. *Macromol. Rapid Commun.* **2007**, *28*, 539–559.
(2) Matyjaszewski, K.; Davis, T. P. *Handbook of Radical Polymerization*; Wiley-Interscience: Hoboken, NJ, 2002.
(3) Matyjaszewski, K.; Xia, J. *Chem. Rev.* **2001**, *101*, 2921–2990.
(4) Patten, T. E.; Xia, J.; Abernathy, T.; Matyjaszewski, K. *Science* **1996**, *272*, 866–868.
(5) Wang, J.-S.; Matyjaszewski, K. *Macromolecules* **1995**, *28*, 7572–7573.
(6) Wang, J.-S.; Matyjaszewski, K. *J. Am. Chem. Soc.* **1995**, *117*, 5614–5615.
(7) Hawker, C. J.; Bosman, A. W.; Harth, E. *Chem. Rev.* **2001**, *101*, 3661–3688.
(8) Georges, M. K.; Veregin, P. M.; Kazmaier, P. M.; Hamer, G. K. *Macromolecules* **1993**, *26*, 2987–2988.
(9) Barner-Kowollik, C.; Davis, T. P.; Heuts, J. P. A.; Stenzel, M. H.; Vana, P.; Whittaker, M. *J. Polym. Sci., Part A: Polym. Chem.* **2003**, *41*, 365–375.
(10) Mayadunne, R. T. A.; Rizzardo, E.; Chiefari, J.; Chong, Y. K.; Moad, G.; Thang, S. H. *Macromolecules* **1999**, *32*, 6977–6980.
(11) The terms macromolecular scaffold, star scaffold, and core all refer to the core of a multiarmed star polymer and are used interchangeably throughout this article.
(12) Hao, X.; Nilsson, C.; Jesberger, M.; Stenzel, M. H.; Malmström, E.; Davis, T. P.; Östmark, E.; Barner-Kowollik, C. *J. Polym. Sci., Part A: Polym. Chem.* **2004**, *42*, 5877–5890.
(13) Jesberger, M.; Barner, L.; Stenzel, M. H.; Malmström, E.; Davis, T. P.; Barner-Kowollik, C. *J. Polym. Sci., Part A: Polym. Chem.* **2003**, *41*, 3847–3861.
(14) Angot, S.; Murthy, K. S.; Taton, D.; Gnanou, Y. *Macromolecules* **1998**, *31*, 7218–7225.
(15) Feng, X.-S.; Pan, C.-Y. *Macromolecules* **2002**, *35*, 2084–2089.
(16) Matyjaszewski, K.; Miller, P. J.; Pyun, J.; Kickelbick, G.; Diamanti, S. *Macromolecules* **1999**, *32*, 6526–6535.
(17) Stenzel-Rosenbaum, M.; Davis, T. P.; Chen, V.; Fane, A. G. *J. Polym. Sci., Part A: Polym. Chem.* **2001**, *39*, 2777–2783.
(18) Chaffey-Millar, H.; Busch, M.; Davis, T. P.; Stenzel, M. H.; Barner-Kowollik, C. *Macromol. Theory Simul.* **2005**, *14*, 143–157.
(19) Chaffey-Millar, H.; Hart-Smith, G.; Barner-Kowollik, C. *J. Polym. Sci., Part A: Polym. Chem.*, **2008**, *46*, 1873–1892.
(20) Chaffey-Millar, H.; Stenzel, M. H.; Davis, T. P.; Coote, M. L.; Barner-Kowollik, C. *Macromolecules* **2006**, *39*, 6406–6419.
(21) The term star–star couple refers to the product formed from combination between two propagating star radicals or between a propagating star radical and a radical carrying core.
(22) Nikitin, A. N.; Castignolles, P.; Charleux, B.; Vairon, J.-P. *Macromol. Rapid Commun.* **2003**, *24*, 778–782.
(23) Asua, J. M.; Beuermann, S.; Buback, M.; Castignolles, P.; Charleux, B.; Gilbert, R. G.; Hutchinson, R. A.; Leiza, J. R.; Nikitin, A. N.; Vairon, J.-P.; van Herk, A. M. *Macromol. Chem. Phys.* **2004**, *205*, 2151–2160.
(24) Junkers, T.; Koo, S. P. S.; Stenzel, M. H.; Davis, T. P.; Barner-Kowollik, C. *Macromolecules* **2007**, *40*, 8906–8912.
(25) Busch, M.; Müller, M. *Macromol. Symp.* **2004**, *206*, 399–418.
(26) Nikitin, A. N.; Hutchinson, R. A. *Macromolecules* **2005**, *38*, 1581–1590.
(27) Boschmann, D.; Vana, P. *Macromolecules* **2007**, *40*, 2683–2693.
(28) Farcet, C.; Belleney, J.; Charleux, B.; Pirri, R. *Macromolecules* **2002**, *35*, 4912–4918.
(29) Postma, A.; Davis, T. P.; Li, G.; Moad, G.; O'Shea, M. S. *Macromolecules* **2006**, *39*, 5307–5318.

(30) Willemse, R. X. E.; van Herk, A. M.; Panchenko, E.; Junkers, T.; Buback, M. *Macromolecules* **2005**, *38*, 5098–5193.
(31) Buback, M.; Hesse, P.; Junkers, T.; Sergeeva, T.; Theis, T. *Macromolecules* **2008**, *41*, 288–291.
(32) Kajiwara, A.; Nanda, A. K.; Matyjaszewski, K. *Macromolecules* **2004**, *37*, 1378–1385.
(33) Sato, E.; Emoto, T.; Zetterlund, P. B.; Yamada, B. *Macromol. Chem. Phys.* **2004**, *205*, 1829–1839.
(34) Yamada, B.; Azukizawa, M.; Yamazoe, H.; Hill, D. J. T.; Pomery, P. J. *Polymer* **2000**, *41*, 5611–5618.
(35) Ahmad, N. M.; Heatley, F.; Lovell, P. A. *Macromolecules* **1998**, *31*, 2822–2827.
(36) Chiefari, J.; Jeffrey, J.; Mayadunne, R. T. A.; Moad, G.; Rizzardo, E.; Thang, S. H. *Macromolecules* **1999**, *32*, 7700–7702.
(37) Plessis, C.; Arzmendi, G.; Alberdi, J. M.; van Herk, A. M.; Leiza, J. R.; Asua, J. M. *Macromol. Rapid Commun.* **2003**, *24*, 173–177.
(38) Arzmendi, G.; Plessis, C.; Leiza, J. R.; Asua, J. M. *Macromol. Theory Simul.* **2003**, *12*, 315–324.
(39) Peck, A. N. F.; Hutchinson, R. A. *Macromolecules* **2004**, *37*, 5944–5951.
(40) The chemical structures shown as products of the termination pathway form as a result of either a combination between two MCRs or a combination between a MCR and another radical carrying species.
(41) Barner-Kowollik, C.; Davis, T. P.; Stenzel, M. H. *Polymer* **2004**, *45*, 7791–7805.
(42) Hanton, S. D. *Chem. Rev.* **2001**, *101*, 527–569.
(43) Jackson, C. A.; Simonsick, W. J. *Curr. Opin. Solid State Mater. Sci.* **1997**, *2*, 661–667.
(44) Jagtap, R. N.; Ambre, A. H. *Bull. Mater. Sci.* **2005**, *28*, 515–528.
(45) Montaudo, G.; Carrocia, S.; Montaudo, M. S.; Puglisi, C.; Samperi, F. *Macromol. Symp.* **2004**, *218*, 101–112.
(46) Peacock, P. M.; McEwan, C. N. *Anal. Chem.* **2006**, *78*, 3957–3964.
(47) Scrivens, J. H.; Jackson, A. T. *Int. J. Mass Spectrom.* **2000**, *200*, 261–276.
(48) Bingöl, B.; Hart-Smith, G.; Barner-Kowollik, C.; Wegner, G. *Macromolecules* **2008**, *41*, 1634–1639.
(49) Szablan, Z.; Lovestead, T. M.; Davis, T. P.; Stenzel, M. H.; Barner-Kowollik, C. *Macromolecules* **2007**, *40*, 26–39.
(50) Lovestead, T. M.; Hart-Smith, G.; Davis, T. P.; Stenzel, M. H.; Barner-Kowollik, C. *Macromolecules* **2007**, *40*, 4142–4153.
(51) Hart-Smith, G.; Lovestead, T. M.; Davis, T. P.; Stenzel, M. H.; Barner-Kowollik, C. *Biomacromolecules* **2007**, *8*, 2404–2415.
(52) Ah Toy, A.; Vana, P.; Davis, T. P.; Barner-Kowollik, C. *Macromolecules* **2004**, *37*, 744–751.
(53) Feldermann, A.; Ah Toy, A.; Davis, T. P.; Stenzel, M. H.; Barner-Kowollik, C. *Polymer* **2005**, *46*, 8448–8457.
(54) Vana, P.; Albertin, L.; Barner, L.; Davis, T. P.; Barner-Kowollik, C. *J. Polym. Sci., Part A: Polym. Chem.* **2002**, *40*, 4032–4037.
(55) Bennet, F.; Lovestead, T. M.; Barker, P. J.; Stenzel, M. H.; Davis, T. P.; Barner-Kowollik, C. *Macromol. Rapid Commun.* **2007**, *28*, 1593–1600.
(56) Gründling, T.; Hart-Smith, G.; Davis, T. P.; Stenzel, M. H.; Barner-Kowollik, C. *Macromolecules* **2008**, *41*, 1966–1971.
(57) Llauro, M.-F.; Loiseau, J.; Boisson, F.; Delolme, F.; Ladavière, C.; Claverie, J. *J. Polym. Sci., Part A: Polym. Chem.* **2004**, *42*, 5439–5462.
(58) Feldermann, A.; Coote, M. L.; Stenzel, M. H.; Davis, T. P.; Barner-Kowollik, C. *J. Am. Chem. Soc.* **2004**, *126*, 15915–15923.
(59) The normal scan types of the LCQ Deca ion trap instrument are contrasted with the ZoomScan scan type, which employs a slower scan rate and has higher than normal resolution.
(60) The ZoomScan scan type of the LCQ Deca ion trap instrument conducts scans at a rate of 1/20th of the normal scan types. These scans are of a higher resolution than normal scans.
(61) For multiply charged products, product peaks would repeat throughout the spectrum at a *m/z* spacing of 86/*n*, where *n* denotes the charge state of the adducts. However, no multiply charged species are observed in the spectra produced in the present study.
(62) Peaks arising from linear chains, ideal stars, and star–star couples are observed outside of the *m/z* regions labeled A, B, and C respectively, but are not dominant outside of these regions.
(63) This column states the DP_n of all oligomeric/polymeric products corresponding to the ion assignment in question which are observed within the full available *m/z* scan range.
(64) As *m/z* errors are already explicitly stated, the first peaks in the experimental and theoretical isotopic peak patterns are aligned (i.e., any *m/z* errors have been corrected for) in order to allow for an easier visual comparison of the two patterns.
(65) Gaida, T. M.; Sopchik, A. E.; Bentrude, W. G. *Tetrahedron Lett.* **1981**, *22*, 4167–4170.
(66) Mordi, R. C.; Walton, J. C. *Tetrahedron* **1993**, *49*, 911–928.
(67) Bentrude, W. G. *Tetrahedron Lett.* **1965**, *40*, 3543–3548.

(68) In cases in which products have been assigned based on peaks in which signal overlap is known to occur, relative abundances are estimated by subtracting the theoretical isotope abundance of the overlapping peak from the peak of interest.

(69) Radical species have been illustrated on the chain ends of MCR containing structures to indicate that the chain ends are still living and may therefore undergo further propagation reactions. The fact that the chain ends are living does not necessarily imply that a propagating radical functionality exists on the chain end at the same time that a MCR exists on the chain backbone.